SCIENTIFIC REPORTS

OPEN

SUBJECT AREAS:
STRUCTURE OF SOLIDS AND LIQUIDS
SOLID-STATE CHEMISTRY
FERROELECTRICS AND MULTIFERROICS

Received
5 August 2013

Accepted
2 October 2013

Published
22 October 2013

Correspondence and requests for materials should be addressed to A.M. (masuno@iis.u-tokyo.ac.jp)

Stabilization of metastable ferroelectric $Ba_{1-x}Ca_xTi_2O_5$ by breaking Ca-site selectivity via crystallization from glass

Atsunobu Masuno[1], Chikako Moriyoshi[2], Teruyasu Mizoguchi[1], Toshihiro Okajima[3], Yoshihiro Kuroiwa[2], Yasutomo Arai[4], Jianding Yu[4], Hiroyuki Inoue[1] & Yasuhiro Watanabe[1]

[1]Institute of Industrial Science, The University of Tokyo, 4-6-1 Komaba, Meguro-ku, Tokyo 153-8505, Japan, [2]Department of Physical Science, Hiroshima University, 1-3-1 Kagamiyama, Higashi-Hiroshima, Hiroshima 739-8526, Japan, [3]Kyushu Synchrotron Light Research Center, 8-7 Yayoigaoka, Tosu, Saga 841-0005, Japan, [4]ISS Science Project Office, Japan Aerospace Exploration Agency, Tsukuba, Ibaraki 305-8505, Japan.

The thermal stability and dielectric and structural properties of ferroelectric $Ba_{1-x}Ca_xTi_2O_5$ ($0 \le x \le 0.30$) prepared by crystallization from glass are investigated. The $Ba_{1-x}Ca_xTi_2O_5$ compounds with $x < 0.10$ are thermally stable phases, while those with $x \ge 0.10$ are metastable phases. The ferroelectric transition temperature drastically decreases from 470 to 220°C with increasing x. Crystal structure analyses reveal that one of two possible Ba sites is occupied by Ca in the stable phase region, while Ca-site selectivity is broken in the metastable phase region. The Ca-site selectivity introduces local distortion and makes the crystal lattice unstable. However, the local distortion is suppressed by the occupancy of Ca into both Ba sites. Accordingly, the metastable ferroelectric phase can be obtained beyond the substitution limit of Ca by crystallization from the glassy state. The stabilization mechanism provides possible wide control of the functionality of materials by expanding the composition range.

Since the discovery of its ferroelectricity in 2003, $BaTi_2O_5$ has attracted considerable interest because of its high ferroelectric transition temperature (T_C) of 470°C, high dielectric constant greater than 20000 in the vicinity of T_C, and transparency to visible light[1–5]. The crystal structure of ferroelectric $BaTi_2O_5$ is monoclinic $C2$ with crystal parameters of $a = 16.9086(1)$ Å, $b = 3.93552(3)$ Å, $c = 9.41498(8)$ Å, $\beta = 103.1006(5)^\circ$, and $Z = 6$[6]. There are three types of TiO_6 octahedra and two Ba sites in the unit cell. Polarization occurs along the b-axis direction. The temperature dependence of bond lengths between cations and neighboring oxygen revealed that the displacement of Ti1 from the center of $Ti1O_6$ along the b-axis is responsible for ferroelectricity[5,6]. Although $BaTi_2O_5$ can be utilized not only as a capacitor, a piezoelectric, but also for its non-linear optical properties, it readily decomposes and cannot be easily obtained as a single phase by a solid-state reaction[7]. This difficulty with synthesis seems to hinder the progress of research toward application.

In 2006, one of the simplest methods for preparing single-phase $BaTi_2O_5$ was developed, where Yu *et al.* fabricated $BaTi_2O_5$ glass by containerless processing and annealed it[8]. They found that $BaTi_2O_5$ glass underwent three crystallization processes, in which two metastable phases (α and β) sequentially appeared at 721 and 745°C, respectively, followed by the crystallization of the stable ferroelectric phase (γ) at 877°C. Single-phase ferroelectric $BaTi_2O_5$ was obtained in several minutes only by annealing glass at around 1000°C. By using this high-quality single-phase sample, charge density distributions of $BaTi_2O_5$ were investigated at room temperature, as well as above and below T_C; the results clearly indicated that the covalent bond nature between Ti1 and O1 along the b-axis was strengthened below T_C[6].

For a ferroelectric material to be widely applicable, it is necessary to control ferroelectric properties by element substitution. In the case of $BaTiO_3$, a large amount of successful substitution engineering made $BaTiO_3$ a crucial component in the semiconductor industry. On the other hand, few reports exist about the effects of substitution on $BaTi_2O_5$. $Ba_{1-x}Sr_xTi_2O_5$ ($0 \le x \le 0.12$) prepared by arc-melting exhibited a slight decrease in T_C[9]. KF-doped $BaTi_2O_5$ synthesized by spark plasma sintering exhibited ferroelectric relaxor behavior[10]. In both cases, the substitution limit of x was rather small, reflecting the instability of the $BaTi_2O_5$ crystal structure. Recently, single-phase ferroelectric $Ba_{0.96}Ca_{0.04}Ti_2O_5$ was obtained by crystallization from glass[11]. Owing to a small amount of Ca substitution, the ferroelectric-phase-transition temperature was significantly lowered by 40°C, which is in complete contrast with the case of Ca substitution in $BaTiO_3$. In addition, Rietveld analysis of synchrotron X-ray

diffraction data revealed that the Ca dopant settles at one of two Ba sites. The occupied site is the Ba1 (4c) site, which is surrounded by a rather distorted oxygen polyhedron, in comparison with the Ba2 (2b) site, as shown in Figure 1[12].

Recently, we reported that $Ba_{1-x}Ca_xTi_2O_5$ glasses could be obtained by containerless processing[13–16]. The glass-forming region is wide and allows x values as high as 0.85. Thus, one can expect that by annealing these glasses, ferroelectric $Ba_{1-x}Ca_xTi_2O_5$ will crystallize over a wider x range. In this study, we report the crystallization of ferroelectric $Ba_{1-x}Ca_xTi_2O_5$ over a wide x range from glasses prepared by containerless processing. Thermal stability and dielectric properties of the ferroelectric phase were investigated. Crystal structure analysis using the Rietveld method was performed on the basis of the synchrotron X-ray diffraction profile, focusing on Ca-site selectivity. Ca-site selectivity was quantitatively evaluated by first-principles calculations. In addition, the local structure around the Ca dopant was investigated by Ca K-edge X-ray absorption near-edge structure (XANES) spectroscopy with the aid of first-principles calculations.

Results

Heat treatment condition. When the glasses were annealed at 1000°C for 10 min, $Ba_{1-x}Ca_xTi_2O_5$ phases were crystallized as a major phase for x ranging from 0 to 0.30, while it was obtained as a minor phase at $x = 0.40$. At a higher Ca content ($x > 0.40$), $Ba_{1-x}Ca_xTi_2O_5$ was not obtained even as a minor phase. Thermal stability at higher temperatures and longer annealing times was found to vary depending on the composition. $Ba_{1-x}Ca_xTi_2O_5$ compounds with a lower Ca content ($0 \le x \le 0.07$) were stable after annealing at 1200°C for 12, 24, 48 h. However, $Ba_{0.90}Ca_{0.10}Ti_2O_5$ decomposed at 1200°C after 12 h, although it was stable at 1100°C for 12 h. At a higher Ca content ($0.12 \le x \le 0.30$), $Ba_{1-x}Ca_xTi_2O_5$ decomposed after 12 h even at 1000°C. These results indicate that the lower Ca content compounds ($0 \le x \le 0.07$) are thermodynamically stable phases, while the higher Ca content compounds ($0.10 \le x \le 0.30$) are metastable phases. Whether it is a stable or metastable phase, it is noted that ferroelectric $Ba_{1-x}Ca_xTi_2O_5$ was obtained up to $x = 0.30$ by crystallization from glass. This value is much higher than that reported for other substituted systems[9,10]. Considering that Sr, as compared with Ca, can easily substitute for Ba, because the ionic radius of Sr^{2+} is closer to that of Ba^{2+} than that of Ca^{2+}, the larger substitution of Ca compared to Sr seems illogical. However, with respect to the stable phase region, the substitution limit of Ca is approximately 0.07. This is reasonably smaller than the value of 0.12 determined for Sr-doped $BaTi_2O_5$. Accordingly, it can be concluded that the crystallization method expands the formation of $BaTi_2O_5$ phases to the metastable region. However, this method cannot be applied to Sr-doped $BaTi_2O_5$, because $Ba_{1-x}Sr_xTi_2O_5$ glasses can only be prepared in the range $0 \le x \le 0.05$ even by containerless processing[15].

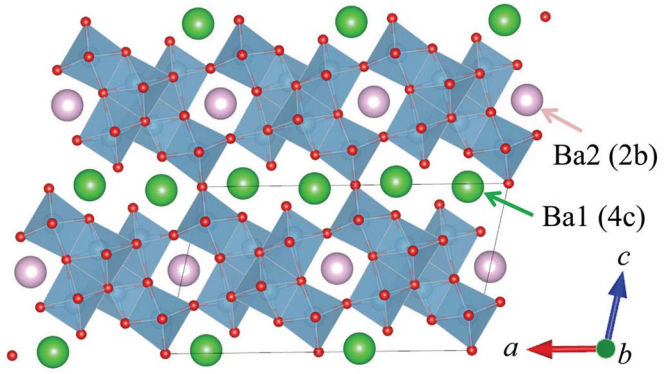

Figure 1 | Crystal structure of ferroelectric $BaTi_2O_5$. Large green and purple spheres represent Ba ions at 2b and 4c sites, respectively. Black lines denote the unit cell.

Dielectric properties. Figure 2 shows the temperature dependence of the dielectric constant ε′ of $Ba_{1-x}Ca_xTi_2O_5$. The heat treatment conditions were 12 h at 1200°C for $0 \le x \le 0.07$ and 10 min at 1000°C for $0.10 \le x \le 0.30$. A characteristic peak at the ferroelectric transition temperature, T_P, is observed for all compositions. The peak sharpness at T_P strongly depended on the Ca content. A sharp peak is observed for the stable phase region ($0 \le x \le 0.07$), as shown in Fig. 2(a), while broader peaks are observed for the metastable phase region ($0.10 \le x \le 0.30$), as shown in Fig. 2(b). The inset of Fig. 2(a) plots the composition dependence of T_P; T_P is found to monotonically decrease with increasing x. Compared to Sr-doped $BaTi_2O_5$, the change in T_P is greater. At $x = 0.05$, T_P decreases by 40°C for Ca-doped $BaTi_2O_5$, while it decreases by 10°C for Sr-doped $BaTi_2O_5$. In the metastable phase region, T_P decreases more drastically to 220°C at $x = 0.30$. This variation in ferroelectric properties between the stable and metastable regions implies difference in their respective crystal structures.

Crystal structure analysis. Figure 3 shows the synchrotron X-ray diffraction profiles of $Ba_{1-x}Ca_xTi_2O_5$ ($0 \le x \le 0.40$). The heat treatment conditions were identical to those utilized for dielectric measurements. No second phase is identified up to $x = 0.20$. A small amount of impurities is observed in the profile of $x = 0.30$. The peaks of the higher Ca content regions are rather broad. This is probably because of the suppression of crystal grain growth caused by lower annealing temperatures and shorter annealing times. The extent of crystallinity is considered to be one of the reasons for the broadening of T_P. At $x = 0.40$, the broad profile prohibits the identification of the

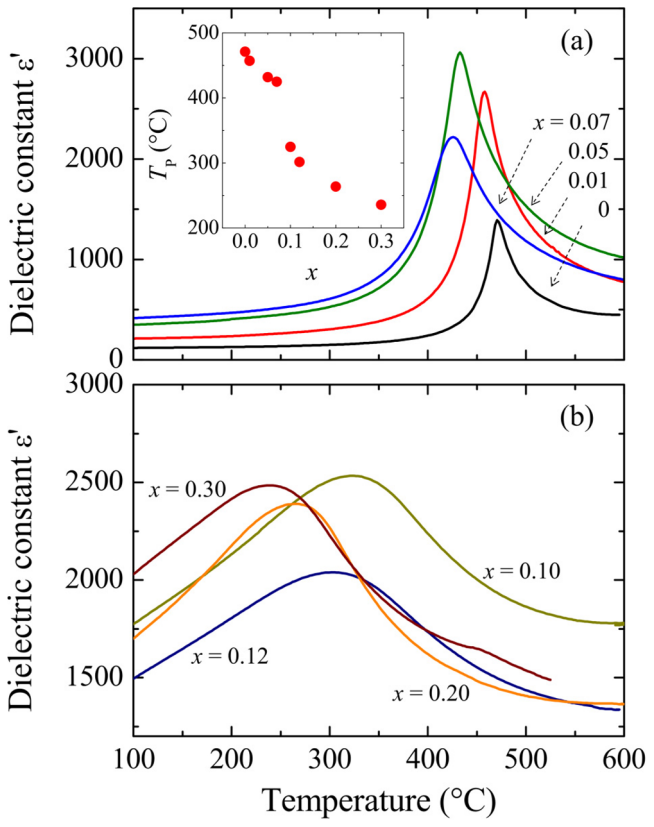

Figure 2 | Graphs of the temperature dependence of the dielectric constant ε′ of $Ba_{1-x}Ca_xTi_2O_5$ for (a) $0 \le x \le 0.07$ and (b) $0.10 \le x \le 0.30$. The inset shows the composition dependence of the peak temperature T_P at the ferroelectric transition.

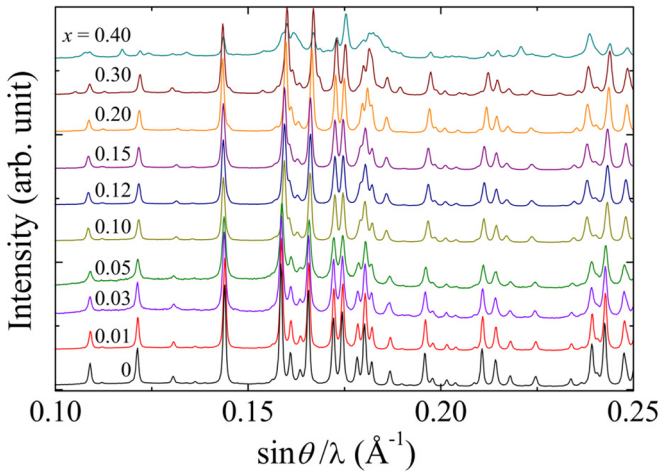

Figure 3 | Synchrotron X-ray diffraction profiles of $Ba_{1-x}Ca_xTi_2O_5$ ($0 \leq x \leq 0.40$, $\lambda = 0.49608(7)$ Å).

crystallized phases. Rietveld analysis was performed on the assumption of the *C*2 space group at $x \leq 0.07$. At $x = 0.10$, the distortion of the Ti1–O6 octahedra is rather small, and therefore, the space group is similar to *C*2/m. At $x = 0.20$ and 0.30, Rietveld analysis cannot distinguish between *C*2 and *C*2/m. Nevertheless, the characteristic peak shown in Fig. 2 supports that the space group of the compound of $x > 0.10$ is certainly non-centrosymmetric *C*2.

Figure 4 shows the composition dependence of the lattice parameters *a*, *b*, and *c*, the bond angle *β*, and the unit cell volume *V*. Although the lattice parameters *a*, *b*, and *c* linearly decreases with increasing *x* in both the stable and metastable regions, a discontinuity is observed at $x = 0.10$. The lattice parameters *a* and *b* decreases over the entire *x* range; however, the lattice parameter *c* decreases with increasing *x* in the stable phase region, jumps at $x = 0.10$, and then decreases with increasing *x* above 0.10. This discontinuity suggests the difference in the effect of Ca doping on the crystal structure between the stable and metastable phase regions. On the other hand, the *V* value gradually decreases as *x* increases to 0.30, suggesting that the Ca^{2+} ion, which has a smaller ionic radius than Ba^{2+}, certainly substitutes for the Ba^{2+} sites. The ratio of the change in the lattice parameter, $\Delta l/l$, is also shown in Fig. 4, which is calculated from the equation $(l_x - l_0)/l_0$, where l_0 corresponds to the lattice parameters a_0, b_0, and c_0 of $BaTi_2O_5$, and l_x corresponds to those of $Ba_{1-x}Ca_xTi_2O_5$. It is apparent that the change of the lattice parameter *b* is greater than those of the lattice parameters *a* and *c*. Large changes in ferroelectric properties are attributed to a large change in the lattice parameter *b*, because the Ti–O bond length along the *b*-axis is considered to be responsible for ferroelectricity in $BaTi_2O_5$. Figure 5 plots the change of T_P as a function of the lattice parameter *b*. The linear relationship between T_P and the lattice parameter *b* is apparent.

XANES spectra. Figure 6 shows the Ca K-edge XANES spectra of $Ba_{1-x}Ca_xTi_2O_5$ and $CaTiO_3$. The calculated spectra are also shown in the figure. First, the Ca K-edge XANES spectrum of $CaTiO_3$ was investigated as a reference to examine the validity of the calculations of the $Ba_{1-x}Ca_xTi_2O_5$ XANES spectra. The experimental spectral fine structure is well reproduced by calculation. The main resonance appears at 4050 eV, corresponding to the main $1s \rightarrow 3p$ transition. It should also be noted that the transition energy can be best reproduced with a relatively small error of $\Delta E = -13.4$ eV ($\Delta E/E = 0.33\%$). In the case of $Ba_{1-x}Ca_xTi_2O_5$, the changes in the spectra clearly depend on the composition, indicating that the local structure of the Ca dopant changes with increasing *x*.

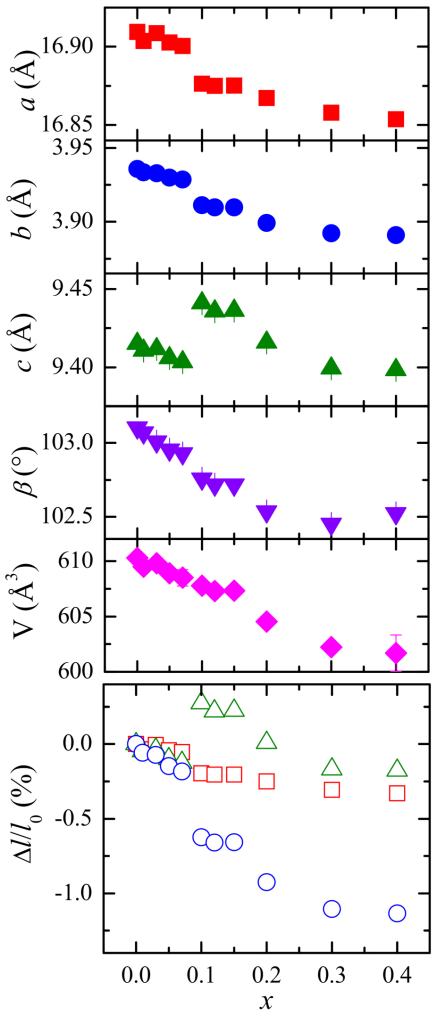

Figure 4 | Composition dependence of the lattice parameters *a*, *b*, *c*, angle *β*, volume *V*, and the ratio of the change of the lattice parameters $\Delta l/l_0$ of $Ba_{1-x}Ca_xTi_2O_5$ ($0 \leq x \leq 0.40$). $\Delta l = l_x - l_0$. l_x presents a lattice parameter at *x*. Squares, circles, and upper triangles correspond to lattice parameters *a*, *b*, and *c*, respectively.

Discussion

The discontinuity of crystal parameters between the stable and metastable regions implies a difference in the mechanism by which Ca is doped into $BaTi_2O_5$. As revealed in our previous study for

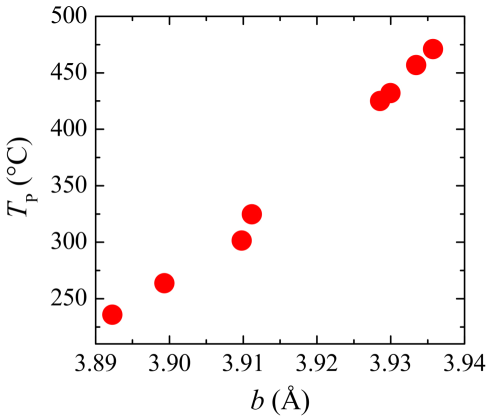

Figure 5 | Ferroelectric peak temperature T_P as a function of the lattice parameter *b* of $Ba_{1-x}Ca_xTi_2O_5$.

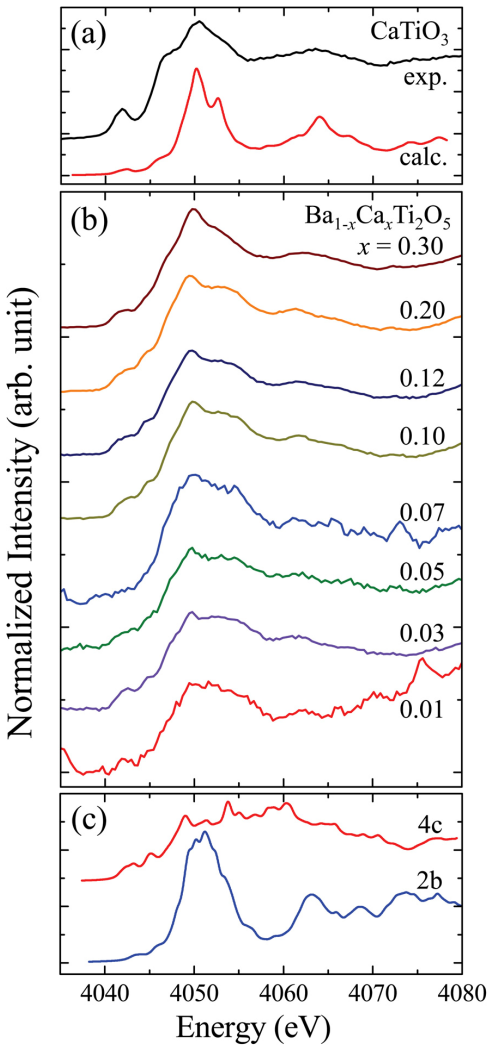

Figure 6 | Ca K-edge X-ray absorption near-edge structure spectra. (a) Experimental and theoretical spectra of $CaTiO_3$. (b) Experimental spectra of $Ba_{1-x}Ca_xTi_2O_5$. (c) Theoretical spectra of $Ba_{1-x}Ca_xTi_2O_5$ with Ca at the Ba1 (4c) site and the Ba2 (2b) site. The theoretical spectra are shifted by $\Delta E = -13.4$ eV ($\Delta E/E = -0.33\%$) for aligning the peak energy of the experimental spectra with that of the theoretical spectra.

$Ba_{0.96}Ca_{0.04}Ti_2O_5$[12], for the stable phase, the site occupancy of Ca at the Ba1 (4c) site is g(Ca1) = 0.056(1), while at the Ba2 (2b) site, it is g(Ca2) = 0, indicating that Ca selectively occupies the Ba1 (4c) site. The composition dependence of g(Ca1) and g(Ca2) is shown in Figure 7(a). The site occupancy g(Ca1) monotonically increases with increasing x, while g(Ca2) is zero in $0 \le x \le 0.7$; however, it increases in the metastable phase region. This indicates that Ca-site selectivity exists in the stable phase region, but it is broken in the metastable region.

The apparent correlation between Ca-site selectivity and the phase stability of Ca-doped $BaTi_2O_5$ can be explained as follows. When the amount of Ca is small, Ca occupies the Ba1 (4c) site. Then, local distortion increases with increasing Ca content. Thus, phase stability decreases, and the ferroelectric phase cannot be obtained as a stable phase for $x \ge 0.10$. The relatively large difference in the ionic radii between Ca and Ba causes a larger local distortion and makes the $BaTi_2O_5$ phase unstable. On the contrary, by crystallization from glass, even a thermally metastable phase can be formed. In the metastable phase, Ca can occupy the Ba2 (2b) and the Ba1 (4c) sites, which in turn suppresses local distortion as compared to the case with Ca site-selectivity. If site selectivity were to be completely eliminated,

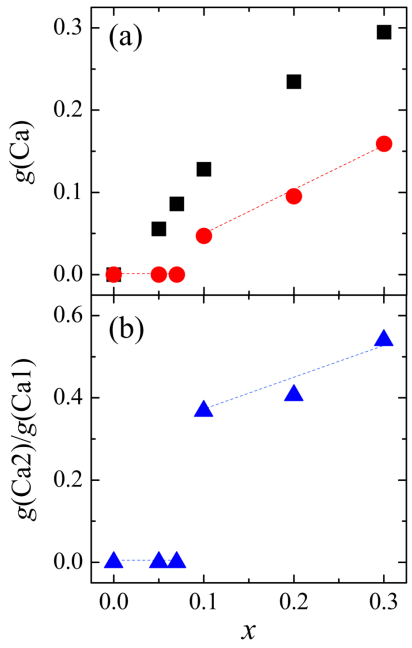

Figure 7 | (a) Composition dependence of the site occupancies of Ca, g(Ca), at the Ba1 site (squares) and at the Ba2 site (circles) in $Ba_{1-x}Ca_xTi_2O_5$. (b) Composition dependence of g(Ca2/g(Ca1).

g(Ca2) should be equal to g(Ca1). However, g(Ca1) is always greater than g(Ca2), and although g(Ca2)/g(Ca1) increases in the metastable phase region, it does not reach 1, as shown in Figure 7(b). The observed differences between g(Ca1) and g(Ca2) indicate that a slight site preference still exists in the metastable region.

Formation energy calculations confirm the quantitative reasonability of site selectivity within the low Ca content region. The formation energy for the substitution of Ca in the Ba1 (4c) site is lower than that for the Ba2 (2b) site by 0.57 eV, suggesting that Ca occupies the Ba1 (4c) site, thereby making the crystal structure more stable than in the case of the Ba2 (2b) site. Figure 8 shows the optimized crystal

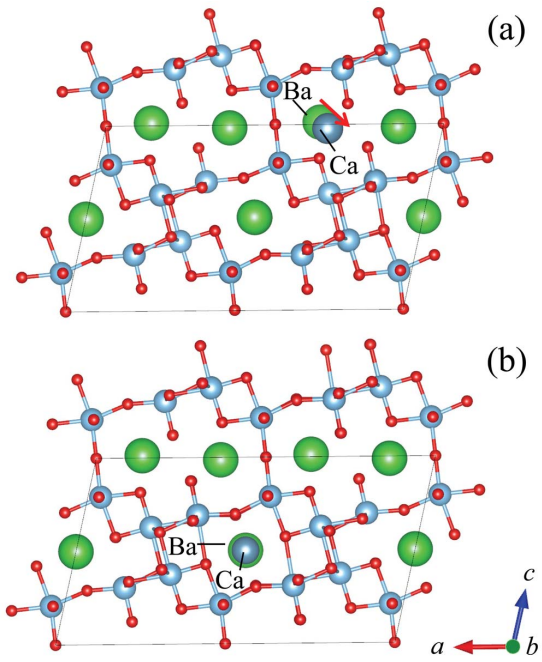

Figure 8 | Optimized crystal structures of Ca-doped $BaTi_2O_5$ at (a) the Ba1 site and (b) the Ba2 site.

structures. The optimized crystal structure of $BaTi_2O_5$ indicates that the Ba environment is spatially larger at the Ba1 (4c) site than at the Ba2 (2b) site. Accordingly, the atomic position of Ca at the Ba1 (4c) site slightly shifts toward open space, and the bond length between Ca and surrounding oxygen becomes 2.5 ~ 3.0 Å, which is close that in $CaTiO_3$, 2.8 Å. On the other hand, the atomic position of Ca at the Ba2 (2b) site is basically same as that of Ba and thus it forms wider variety of Ca-O bonding, 2.2 ~ 3.3 Å. This suggests that Ca-site selectivity occurs because the environment of the Ba1 (4c) site has space to relax the local structure, thereby allowing for a decrease in the formation energy after substitution by Ca as compared to the Ba2 (2b) site. However, with increasing x, structural distortion increases around the Ca dopant at the Ba1 (4c) site, and the stability of the crystal structure decreases. As a result, over $x = 0.10$, the distorted structure caused by Ca-site selectivity cannot be maintained.

As shown in Fig. 6, the XANES spectra at a higher Ca content contains a sharp peak, while at $x \leq 0.07$, the spectra is broad. Compared to the calculated XANES spectra in the case where Ca occupies the Ba1 (4c) and the Ba2 (2b) sites, the spectra of $x \leq 0.07$ are similar to that of the Ba1 (4c) site, while at $x \geq 0.10$, the spectra are similar to that of a mixture of Ba1 (4c) and Ba2 (2b) sites. These results strongly support that Ca-site selectivity is suppressed for $x \geq 0.10$ and that both Ba sites are occupied by the Ca dopant.

In summary, ferroelectric $Ba_{1-x}Ca_xTi_2O_5$ ($0 \leq x \leq 0.30$) compounds were prepared by crystallization from glass. The compounds with $x < 0.10$ are thermodynamically stable, while those of $x \geq 0.10$ are metastable. As x increases, the ferroelectric transition temperature drastically decreases to 220°C in the metastable region. The structural parameters obtained from synchrotron X-ray diffraction measurements, as well as ferroelectric properties, discontinuously change, crossing the boundary between the stable and metastable phase regions. Rietveld analyses revealed that Ca occupies one of two Ba sites in the stable phase region, while Ca-site selectivity was broken in the metastable phase region. First-principles calculations of the formation energy support Ca-site selectivity in the lightly doped region. Furthermore, Ca K-edge X-ray absorption near-edge structure spectra experimentally and theoretically demonstrated that the local structure around Ca changed depending on Ca-site selectivity. These results indicate distortion of the local structure around the Ca dopant in the stable region and decrease in the phase stability with increasing Ca content under conditions of Ca-site selectivity. On the other hand, by crystallization from the thermally non-equilibrium glassy state, Ca can occupy both Ba sites, thereby suppressing local structural distortions that cause decomposition at a higher Ca content. The strong correlation observed between Ca-site selectivity and phase stability indicates that there are various thermodynamically comparable phases in the composition of $Ba_{1-x}Ca_xTi_2O_5$. As a result, these phases can be obtained by adjusting their energy balance using various synthetic approaches. The proposed stability mechanism via crystallization from glass provides the possibility to produce functional materials over a wide composition range.

Methods

Sample preparation. High-purity $BaCO_3$, $CaCO_3$, and TiO_2 powders were stoichiometrically mixed in the composition of $Ba_{1-x}Ca_xTi_2O_5$ ($0 \leq x \leq 0.40$). The mixed powders were sintered at 1000°C for 12 h in air. Sintered samples weighing approximately 10–20 mg were used as targets in an aerodynamic levitation (ADL) furnace. A 100-W CO_2 laser was applied to the melt. The melt was levitated by oxygen gas. The details of the ADL technique are described in previous reports[13–16]. For all compositions, glass formation was confirmed by X-ray diffraction measurements with Cu $K\alpha$ radiation. The chemical composition of glasses was analyzed by energy-dispersive X-ray fluorescence spectroscopy (Rigaku XRF JSX-3100RII). The deviation of the resulting composition from the target composition was less than 0.2%. Depending on the glass composition, the diameter of the spherically shaped solidified glasses was approximately 1.2–3.5 mm. With increasing Ca content, glass stability was enhanced, and larger-sized glass samples were obtained[15,16].

The spherical glasses obtained were annealed above 1000°C and then crystallized. Although the appropriate heat treatment conditions for the crystallization of the ferroelectric phase were varied with chemical composition, Ca-doped $BaTi_2O_5$ was obtained in the range of x up to 0.40, which was confirmed by X-ray diffraction measurements with Cu $K\alpha$ radiation.

Dielectric property measurement. The temperature dependence of the dielectric properties of $Ba_{1-x}Ca_xTi_2O_5$ was measured using an impedance analyzer with ac frequencies up to 1 MHz. Both sides of the crystallized spherical glasses were sliced to form a 0.5-mm-thick disk. Gold electrodes were sputtered on both faces, and silver paste used to connect silver wires to the electrodes. The temperature was increased to 700°C at a rate of 2°C/min under oxygen gas.

Crystal structure analysis. To obtain the crystal structure parameters of $Ba_{1-x}Ca_xTi_2O_5$, synchrotron X-ray powder diffraction measurements were carried out using a large Debye–Scherrer camera with an imaging plate installed at BL02B2 in SPring-8[17]. To obtain homogeneous intensity distribution in the Debye–Scherrer powder ring, the annealed samples were ground in an agate mortar, and a powdered sample having homogeneous granularity was prepared by the precipitation method. The powdered sample was sealed in a quartz capillary with an internal diameter of 0.2 mm. The synchrotron radiation energy was 25 keV ($\lambda = 0.49499(5)$ Å). Rietveld analysis was applied to the diffraction intensity data in the range of $\sin\theta/\lambda < 0.96$ Å^{-1} ($d > 0.52$ Å). The reported structural parameters of $BaTi_2O_5$ were used as the starting parameters for Rietveld analysis[6].

Formation energy calculation. The formation energies of the two structural models of Ca-doped $BaTi_2O_5$ were evaluated by first-principles calculations. In one structural model, Ca occupies the Ba1 (4c) site, while in the other, it occupies the Ba2 (2b) site. In the calculations, a supercell consisting of $1 \times 3 \times 1$ optimized unit cells was employed. Structural optimizations were performed by employing the projector-augmented wave method[18], implemented using the VASP code[19–21]. A Ca ion was doped into a Ba site in the constructed supercell, and the local structure around the Ca dopant was optimized under fixed volume conditions until the residual force decreased below 0.05 eV/Å. The Γ-point was selected for k-point sampling. The generalized gradient approximation proposed by Perdew–Burke–Ernzerhof (GGA-PBE) was used as an exchange-correlation functional, and the plane-wave cutoff energy was set to 350 eV[22–24].

Local structure analysis. The local structure around the Ca dopant was investigated by Ca K-edge XANES spectroscopy by a combination of experiment and simulation. The experimentally obtained XANES spectra of Ca-doped $BaTi_2O_5$ were acquired in the fluorescence-yield mode using synchrotron radiation from a bending magnet of the 1.4-GeV storage ring at BL11 in SAGA Light Source[25,26]. The spectra were measured with a fixed-exit double-crystal monochromator employing Si (111) planes and a rhodium-coated bent cylindrical mirror. An ionization chamber filled with a mixed gas of 70% He and 30% N_2 was inserted into the optical path to monitor photon flux. The emitted X-ray fluorescence from the specimens was measured by a silicon drift detector. As a reference, the spectrum of $CaTiO_3$ was also obtained in the fluorescence-yield mode. All measurements were performed in air at room temperature.

Simulation of XANES spectra. Simulations of Ca K-edge XANES spectra of Ca-doped $BaTi_2O_5$ and $CaTiO_3$ were carried out by using the full-potential linearized augmented plane wave plus local orbitals (APW+ lo) package, WIEN2k[27]. The optimized structures of the two models of Ca-doped $BaTi_2O_5$ obtained by formation energy calculations were applied to the XANES spectra calculations. GGA-PBE was employed as an exchange-correlation functional. All electrons up to 2p, 2p, and 4d were treated as core electrons for Ca, Ti, and Ba, respectively, while only 1s electrons were treated as core electrons for O. The muffin-tin radius, R_{MT}, was set to 1.7, 1.7, 1.55, and 2.5 bohr for Ti, O, Ca, and Ba, respectively. The product of the muffin-tin radius and the maximum reciprocal space vector K_{max}, i.e., the plane-wave cutoff, $R_{MT} \times K_{max}$, was fixed at 6.0 bohr Ry$^{1/2}$. Relativistic effects were completely introduced for the core electrons by solving the Dirac equation, while valence electrons were treated within scalar relativistic approximations. The theoretical XANES spectra were obtained by calculating transition matrix elements between the core state and conduction bands. Core–hole effects were fully considered in the present calculations by removing one electron from the Ca 1s orbital of interest and putting one additional electron at the bottom of the conduction band. Nine k-points were selected for Brillouin-zone integrations. Each of the calculated spectra was broadened by a Gaussian function of $\Gamma = 1.0$ eV full-width at half-maximum. The XANES calculation details are described elsewhere[28].

1. Akishige, Y., Fukano, K. & Shigematsu, H. New Ferroelectric $BaTi_2O_5$. *Jpn. J. Appl. Phys.* **42**, L946–L948 (2003).
2. Akashi, T., Iwata, H. & Goto, T. Preparation of $BaTi_2O_5$ Single Crystal by a Floating Zone Method. *Mater. Transactions* **44**, 802–804 (2003).
3. Kimura, T. *et al.* A ferroelectric barium titanate, $BaTi_2O_5$. *Acta Crystallogr. Sect. C* **59**, i128–i130 (2003).
4. Akishige, Y., Shigematsu, H., Kitahara, A. & Takahashi, I. Phase transition of new ferroelectric $BaTi_2O_5$. *J. Korean Phys. Soc.* **46**, 24–28 (2005).
5. Shigematsu. *et al.* Neutron powder diffraction study of the phase transition in $BaTi_2O_5$. *Ferroelectrics* **346**, 43–48 (2007).
6. Moriyoshi, C. *et al.* Charge Density Study on Phase Transition in $BaTi_2O_5$ Ferroelectric. *Jpn. J. Appl. Phys.* **48**, 09KF06 (2009).

7. Zhu, N. & West, A. R. Formation and Stability of Ferroelectric $BaTi_2O_5$. *J. Am. Ceram. Soc.* **93**, 295–300 (2010).
8. Yu, J. *et al.* Fabrication of $BaTi_2O_5$ glass-ceramics with unusual dielectric properties during crystallization. *Chem. Mater.* **18**, 2169–2173 (2006).
9. Yue, X. Y., Tu, R. & Goto, T. AC impedance analysis on b-axis oriented $Ba_{1-x}Sr_xTi_2O_5$ prepared by an arc-melting method. *J. Ceram. Soc. Jpn.* **115**, 648–653 (2007).
10. Xu, J. & Akishige, Y. Relaxor in KF-doped $BaTi_2O_5$ ceramics by spark plasma sintering. *Appl. Phys. Lett.* **92**, 052902 (2008).
11. Moriyoshi, C., Kuroiwa, Y., Masuno, A. & Inoue, H. Site-Selective Calcium Substitution in $BaTi_2O_5$: Effect on the Crystal Structure and the Ferroelectric Phase Transition. *J. Phys. Soc. Jpn.* **81**, 014706 (2012).
12. Momma, K. & Izumi, F. VESTA 3 for three-dimensional visualization of crystal, volumetric and morphology data. *J. Appl. Crystallogr.* **44**, 1272–1276 (2011).
13. Masuno, A., Inoue, H., Yu, J. & Arai, Y. Refractive index dispersion, optical transmittance, and Raman scattering of $BaTi_2O_5$ glass. *J. Appl. Phys.* **108**, 063520 (2010).
14. Masuno, A., Kikuchi, Y. & Inoue, H. Giant Second Harmonic Generation from Metastable $BaTi_2O_5$. *Appl. Phys. Express* **4**, 042601 (2011).
15. Masuno, A., Inoue, H., Arai, Y. & Yu, J. Structural-relaxation-induced high refractive indices of $Ba_{1-x}Ca_xTi_2O_5$ glasses. *J. Mater. Chem.* **21**, 17441–17447 (2011).
16. Masuno, A. *et al.* Giant dielectric response with metastable phase crystallization from $Ba_{1-x}Ca_xTi_2O_5$ glasses. *J. Non-Cryst. Solids* **358**, 3505−3509 (2012).
17. Nishibori, E. *et al.* The large Debye–Scherrer camera installed at SPring-8 BL02B2 for charge density studies. *Nucl. Instrum. Methods Phys. Res., Sect. A* **467–468**, 1045–1048 (2001).
18. Blöchl, P. E. Projector augmented-wave method. *Phys. Rev. B* **50**, 17953–17979 (1994).
19. Kresse, G. & Hafner, J. Ab initio molecular dynamics for liquid metals. *Rev. B* **47**, 558–561 (1993).
20. Kresse, G. & Furthmuller, J. Efficient iterative schemes for ab initio total-energy calculations using a plane-wave basis set. *Phys. Rev. B* **54**, 11169–11186 (1996).
21. Kresse, G. & Joubert, D. From ultrasoft pseudopotentials to the projector augmented-wave method. *Phys. Rev. B* **59**, 1758–1775 (1999).
22. Perdew, J. P. & Wang, Y. Accurate and simple analytic representation of the electron-gas correlation energy. *Phys. Rev. B* **45**, 13244–13249 (1992).
23. Perdew, J. P., Burke, K. & Ernzerhof, M. Generalized Gradient Approximation Made Simple. *Phys. Rev. Lett.* **77**, 3865–3868 (1996).
24. Perdew, J. P., Burke, K. & Ernzerhof, M. *Phys. Rev. Lett.* **78**, 1396–1396 (1997).
25. Okajima, T. *et al.* The Design and Performance of Beamline BL15 at SAGA Light Source. *AIP Conference Proceedings* **879**, 820–823 (2007).
26. Okajima, T., Yasukawa, K. & Umesaki, N. Local structure of Ca dopant in $BaTiO_3$ by Ca K-edge X-ray absorption near-edge structure and first-principles calculations. *J. Electron Spectrosc. Relat. Phenom.* **180**, 53–57 (2010).
27. Blaha, A., Schwarz, K., Madsen, G., Kvascka, D. & Luitz, J. WIEN2k, An Augmented Plane Wave + Local Orbital Program for Calculating Crystal Properties, Vienna University of Technology, Vienna, 2001.
28. Mizoguchi, T., Olovsson, W., Ikeno, H. & Tanaka, I. Theoretical ELNES using one-particle and multi-particle calculations. *Micron* **41**, 695–709 (2010).

Acknowledgments

Synchrotron X-ray powder diffraction experiments were carried out at BL02B2 in SPring-8 with the approval of the Japan Synchrotron Radiation Research Institute (Nos. 2008B0096, 2008B1040, and 2009A0084). The X-ray absorption experiment using synchrotron radiation was performed at BL11 of the SAGA-LS (No. 100999PT). This study was partially supported by Nippon Sheet Glass Foundation, Iketani Science and Technology Foundation, Tokuyama Science Foundation. AM, HI, and TM are also supported by the Ministry of Education, Culture, Sports, Science and Technology of Japan (Nos. 19750174, 23750236, and 25410236), (No. 21550185), and (Nos. 19053001, 22686059, 23656395, and 25106003), respectively. Some simulations were performed by the supercomputing system in the Institute of Solid State Physics, The University of Tokyo.

Author contributions

A.M. organized the research and wrote the manuscript. A.M., C.M., T.M., T.O. and Y.K. conducted the experiments and analyzed the results. Y.A., J.Y., H.I. and Y.W. discussed the results. All authors reviewed the manuscript.

Additional information

Competing financial interests: The authors declare no competing financial interests.

How to cite this article: Masuno, A. *et al.* Stabilization of metastable ferroelectric $Ba_{1-x}Ca_xTi_2O_5$ by breaking Ca-site selectivity via crystallization from glass. *Sci. Rep.* **3**, 3010; DOI:10.1038/srep03010 (2013).